Supplementary information for

Time-Lagged Climate and Vegetation Feedbacks Intensify Seasonal CO2 Exchange in High Latitudes

Naixin Fan, Wolfgang Buermann, Stephen Sitch, Christian Rodenbeck, Kirsten Thonicke, Markus Drüke, Matthias Forkel

Corresponding author: naixin.fan@icloud.com

The covariation between large-scale atmospheric circulation and CO_2 amplitude

To assess the influence of large-scale atmospheric circulation on CO_2 amplitude, we analyzed three major climate indices: the North Atlantic Oscillation (NAO), the Arctic Oscillation (AO), and the El Niño–Southern Oscillation (ENSO). Each of these indices is linked to interannual variability in atmospheric circulation patterns, which can influence climate conditions across the high latitudes. We find that interannual fluctuations in October AO, October NAO, and April ENSO exhibit moderate correlations with CO_2 amplitude (Rd = 0.48, 0.47, and –0.43, respectively), each with a 4-year time lag (Fig. S13). These results suggest that changes in large-scale atmospheric circulation can precede shifts in CO_2 amplitude by several years, potentially through their downstream effects on temperature, moisture availability, and ecosystem processes. However, the absence of significant long-term trends in these indices during the analyzed months indicates that while they may modulate interannual variability, they are unlikely to be the primary drivers of the long-term amplification in CO_2 amplitude.

In contrast, August NAO displays both a significant downward trend from 1980 to 2018 and a strong negative correlation with CO_2 amplitude at a 1-year lag (R_0 = –0.65, R_d = –0.55; $p < 0.01$). This relationship implies that weakened summer NAO conditions—associated with suppressed westerlies and increased likelihood of hotter and drier conditions over northern Eurasia—are linked to elevated CO_2 amplitude in the subsequent year. Further analysis shows that August NAO in year N–1 is correlated with multiple environmental variables, including May soil moisture in year N–1 (R_0 = 0.47, R_d = 0.42; $p < 0.01$), tree canopy cover in year N–1 (R_0 = -0.51, R_d = -0.49; $p < 0.01$), freeze date in year N–1 (R_0 = -0.43, R_d = -0.36; $p < 0.01$), May temperature in year N–2 (R_0 = -0.50, R_d = -0.36; $p < 0.01$). These linkages suggest that the NAO may modulate hydroclimate conditions relevant to carbon cycling through indirect effect in conjunction with other, more dominant factors.

Interconnection among land cover change, fire, and CO_2 amplitude

To assess the role of land cover change in modulating CO_2 amplitude, we examined long-term global tree canopy cover data ($\geqslant$5 m in height) from 1982 to 2015, representing peak growing season vegetation structure (Song et al., 2018). Our analysis reveals a positive correlation (R_d = 0.47) between tree canopy cover and CO_2 amplitude with a 1-year lag, indicating that years with higher tree canopy extent are associated with increased CO_2 amplitude in the subsequent year (Fig. S14). This result supports previous findings that compositional shifts in vegetation—particularly the expansion of tree cover over grasslands and shrubs—can influence seasonal carbon exchange dynamics (Zeng et al., 2014; Forkel et al., 2016; Kondo et al., 2018).

To further test this hypothesis, we analyzed long-term trends in short vegetation cover ($\leqslant$5 m in height) over the same period. We find a negative correlation (R_d = –0.46) between short vegetation cover and CO_2 amplitude, also with a one-year lag, suggesting that increased cover of shrubs and grasses is associated with lower seasonal CO_2 amplitude. Additionally, a strong negative correlation (R_d = –0.58) between year-to-year changes in tree canopy and short vegetation cover (with zero-year lag) indicates a competitive relationship between these two vegetation types across the circumpolar region. Together, these findings suggest that vegetation compositional changes play a significant role in modulating the interannual variability of CO_2 amplitude.

To evaluate fire's contribution to CO_2 amplitude variability, we analyzed data from the Global Fire Emissions Database (GFED4; 1997–2018). August fire emissions exhibit a strong negative correlation with CO_2 amplitude (R_d = –0.78) at a four-year lag (Fig. S15), suggesting that fire disturbances may influence carbon exchange through legacy effects on vegetation structure and ecosystem recovery. However, the relatively short temporal coverage of the GFED4 dataset—approximately two decades shorter than other datasets used in this study—limits confidence in attributing multidecadal trends in CO_2 amplitude to fire activity. As such, while fire may contribute substantially to interannual variability, its role in long-term amplification remains uncertain.

Evaluation of Correlation Differences Between GPP, TER, and CO_2 Amplitude

To assess whether TER exhibits a stronger association with CO_2 amplitude than GPP, we compared correlation strengths across the ensemble of the TRENDY models, treating each model as an independent estimate of the underlying relationship.

Because correlation coefficients are bounded between −1 and 1 and not normally distributed, we converted each correlation (Table S1 and S4) to a normal scale using Fisher's transform:

$$z_i = \frac{1}{2}\ln\left(\frac{1+r_i}{1-r_i}\right)$$

This transformation allows the across-model distribution of correlation strengths to be treated as approximately normal, enabling ensemble-level statistical comparison.

To test whether respiration correlates more strongly with CO_2 amplitude than photosynthesis, we computed the paired difference in transformed correlations for each model:

$$\Delta z_i = z_{TER,i} - z_{GPP,i}$$

These ten values represent independent cross-model estimates of the correlation difference for a given month. We then tested whether the ensemble mean difference is significantly greater than zero using a paired t-test:

$$t = \frac{\overline{\Delta z}}{SD(\Delta z)/\sqrt{n}}$$

For the month May and October, we obtained:

$$\overline{\Delta z_{May}} = 0.085$$
$$\overline{\Delta z_{Oct}} = 0.122$$

$$SD(\Delta z_{May}) = 0.165$$
$$SD(\Delta z_{Oct}) = 0.064$$

At the degree freedom of 9, t = 1.61, corresponding to **p = 0.14** for May. For October, t = 5.82, corresponding to **p < 0.001**.

We estimated 95% confidence intervals for the ensemble-mean differences in transformed correlations as:

$$\overline{\Delta z} \pm 1.96 \times \frac{SD(\Delta z)}{\sqrt{n}}$$

This yields:

$$\Delta z_{May} = [-0.03, 0.20]$$
$$\Delta z_{Oct} = [0.08, 0.17]$$

Although the May interval skewed towards positive values, the ensemble does not show a statistically significant difference between GPP and TER correlations in that month ($p = 0.14$). By contrast, the October statistics show a significant ($p<0.001$), ensemble-wide tendency for respiration to correlate more strongly with CO_2 amplitude than photosynthesis.

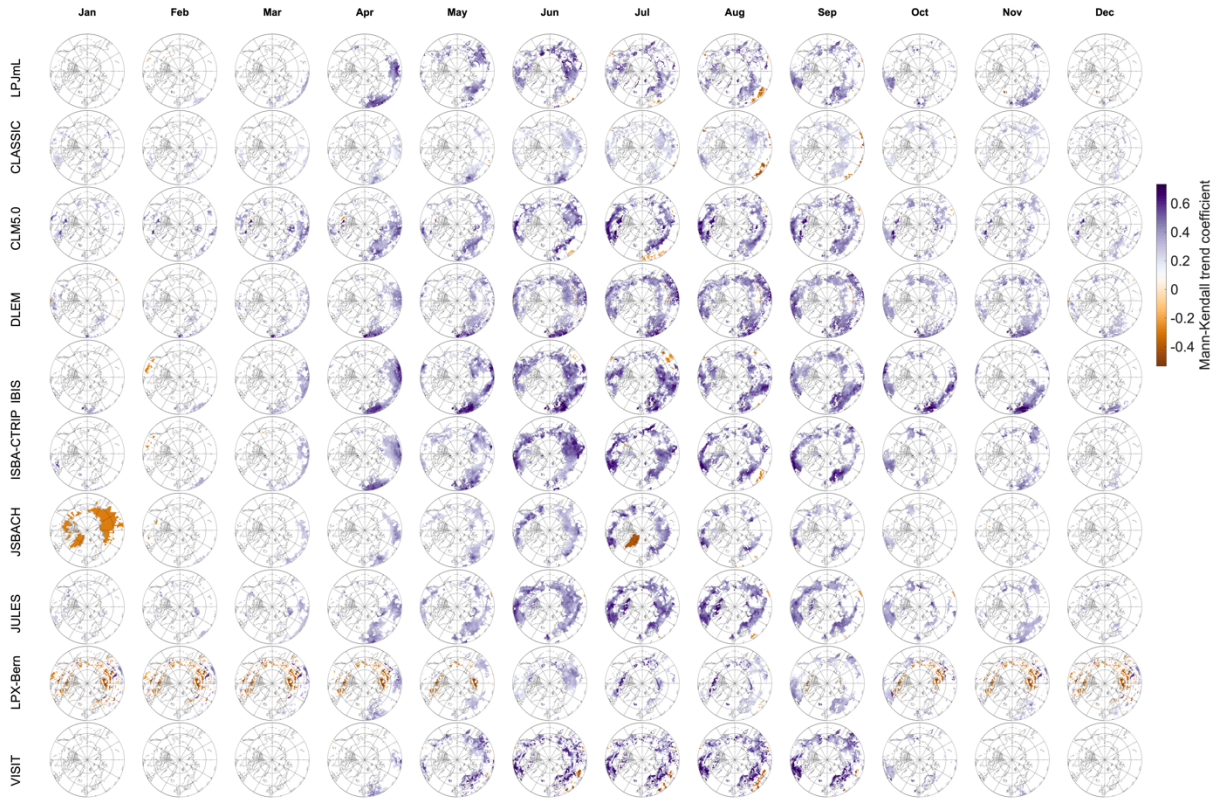

Fig. S1. Long-term trend of GPP for each individual month (January to December) at the grid-cell level, derived from selected TRENDY models from 1980 to 2018. Long-term trends are analyzed using the Mann-Kendall test. Grid cells shown in purple indicate a statistically significant ($p < 0.05$) increasing trend, while those in orange indicate a decreasing trend.

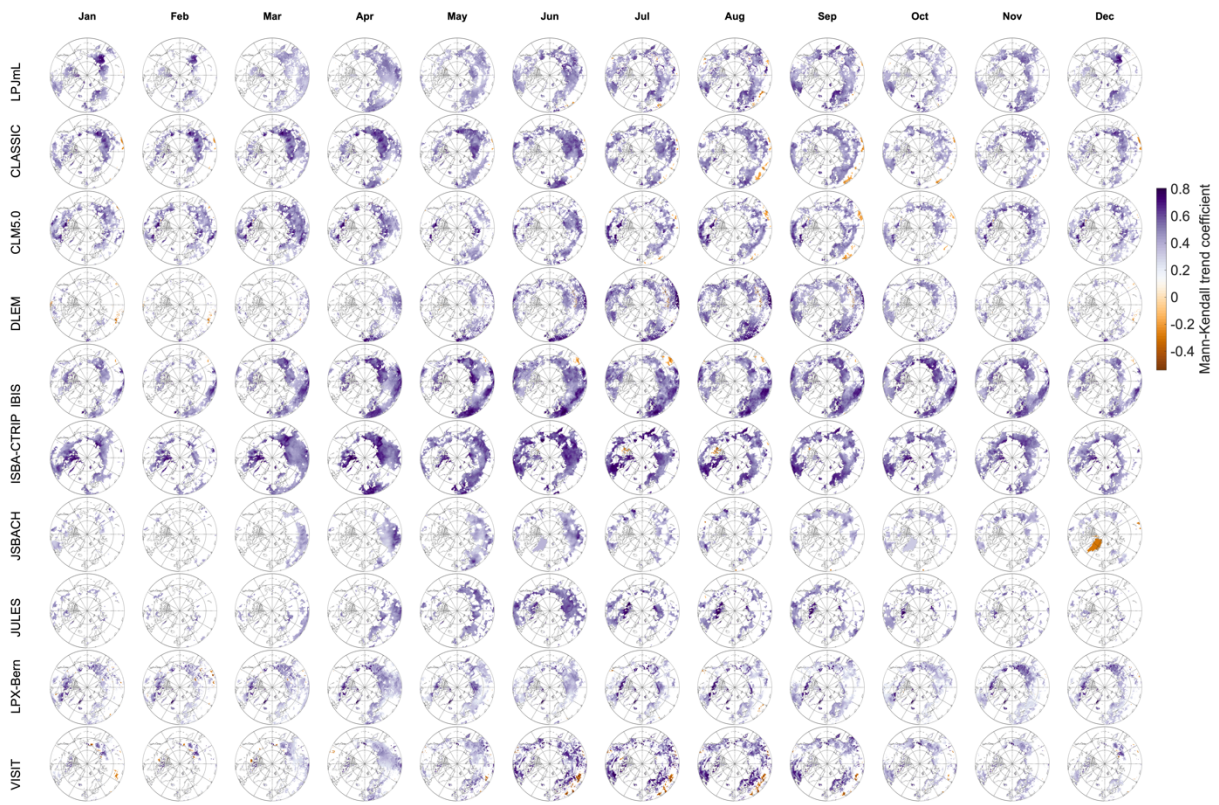

Fig. S2. Same as Figure S1 except for TER instead of GPP.

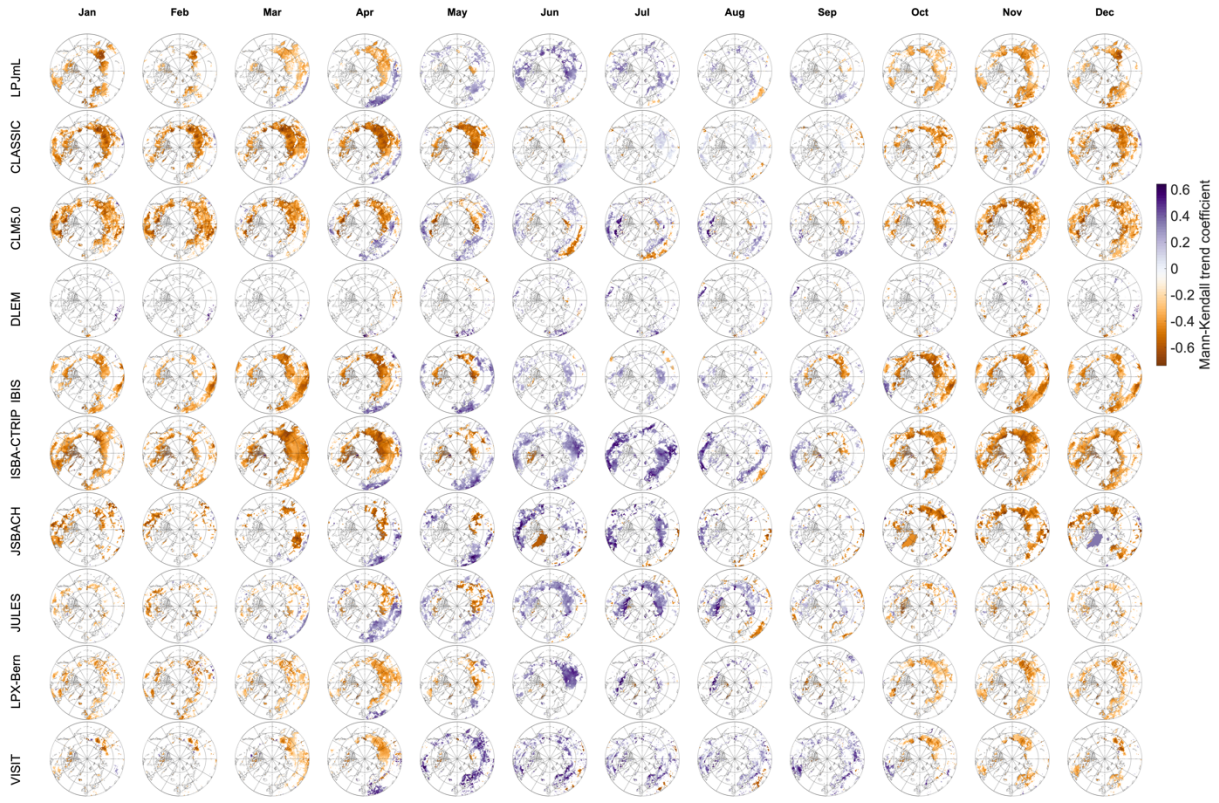

Fig. S3. Same as Figure S1 except for NEP instead of GPP.

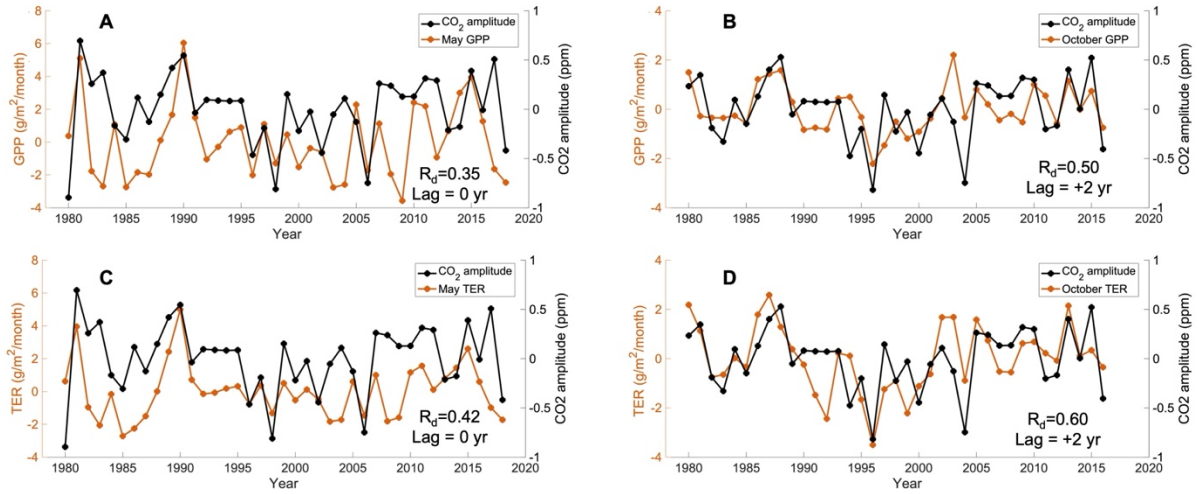

Fig. S4. Interannual variability in CO2 amplitude (Barrow), GPP, and TER from 1980 to 2018. Time series of GPP and TER are derived from the average of selected TRENDY models. Note that CO2 amplitude time series in subplot **B, D** is shifted 2 years back as a 2-year time lag is detected between CO2 amplitude and October GPP/TER. All time series are detrended to isolate interannual variability from long-term trend.

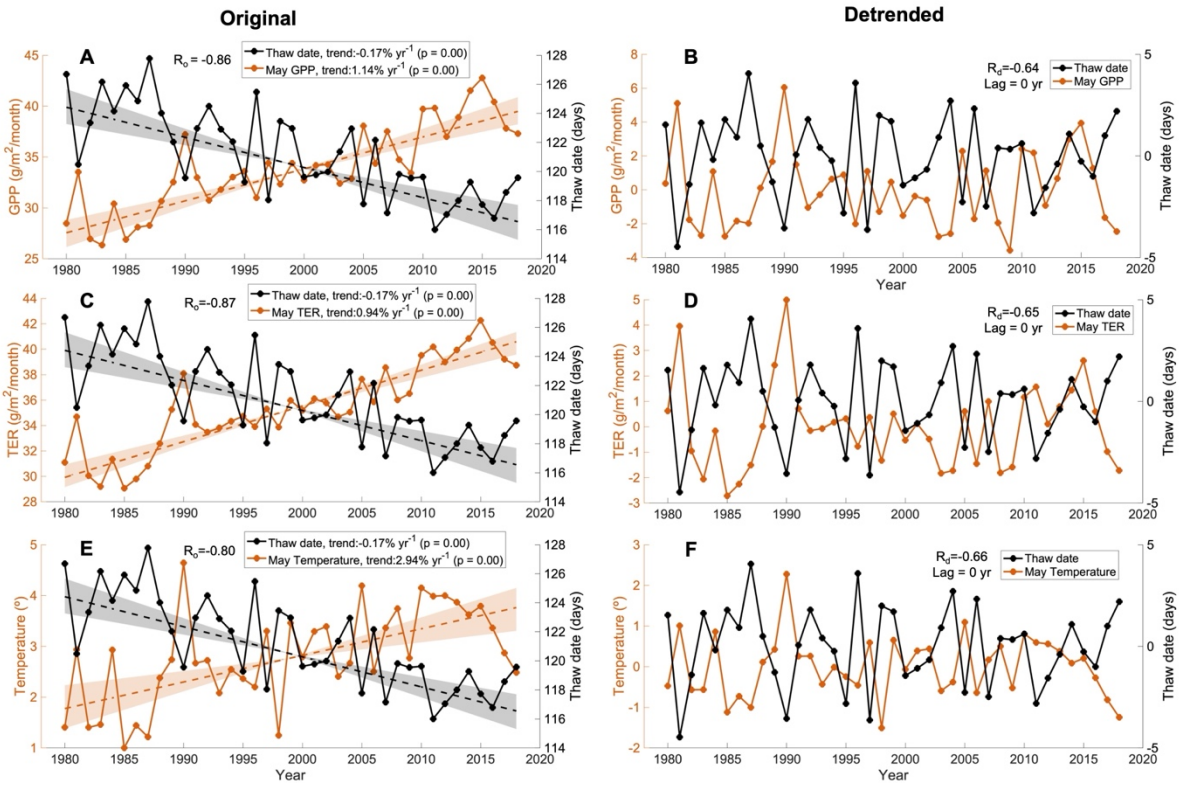

Fig. S5. Covariation between thaw date and May GPP, TER, and temperature from 1980 to 2018. Left panels show the original time series with fitted linear trends (Mann-Kendall test); right panels show the corresponding detrended time series with long-term trends removed. Negative and positive lag times indicate that variable A leads or lags variable B, respectively, while a lag time of zero denotes no detectable legacy effect.

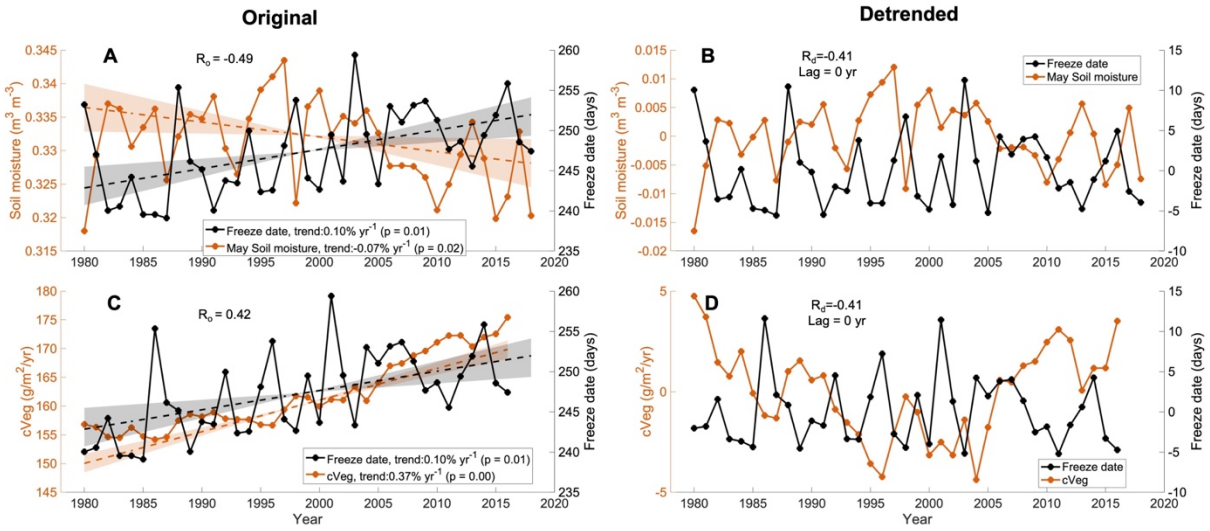

Fig. S6. Same as Fig. S5, except showing the covariation between freeze date and soil moisture (A, B) and between freeze date and vegetation carbon stock (C, D).

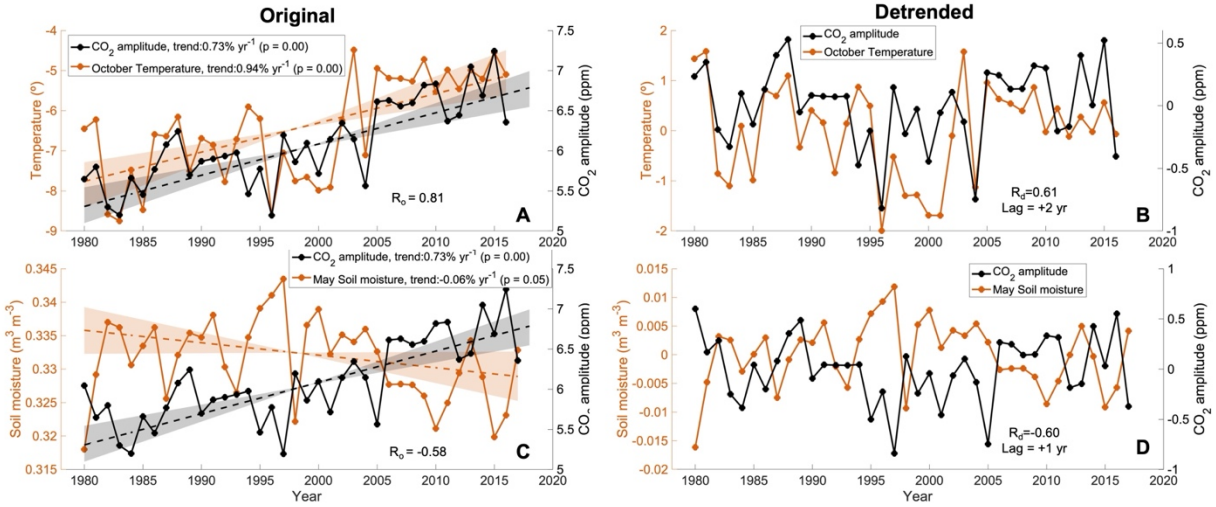

Fig. S7. Same as Fig. S5, except showing the covariation between CO_2 amplitude and October temperature (A, B) and between CO_2 amplitude and May soil moisture (C, D).

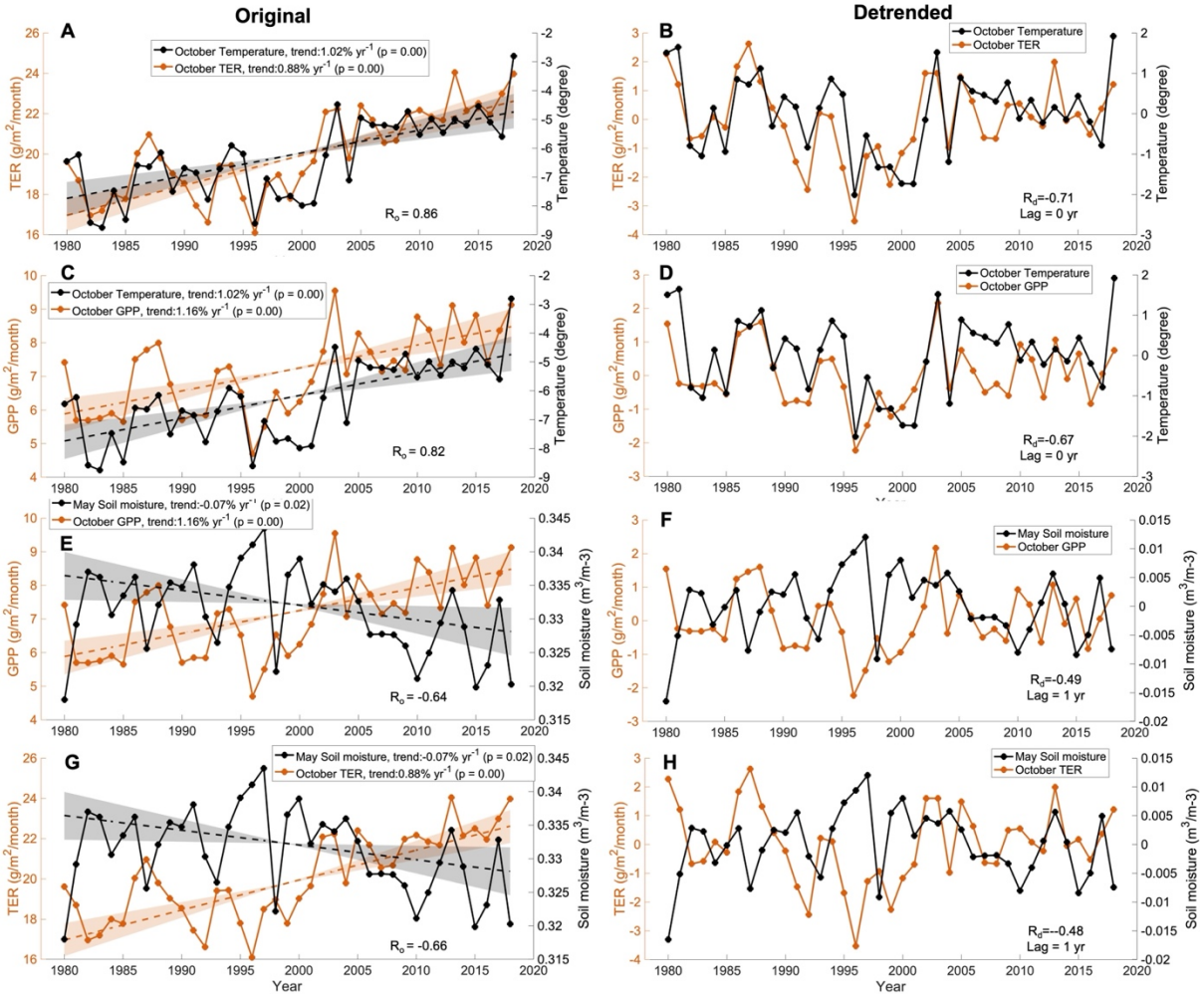

Fig. S8. Same as Fig. S5, except showing the covariation between October TER and October temperature (A, B), October GPP and October temperature (C, D), October GPP and May soil moisture (E, F), October TER and May soil moisture (G, H).

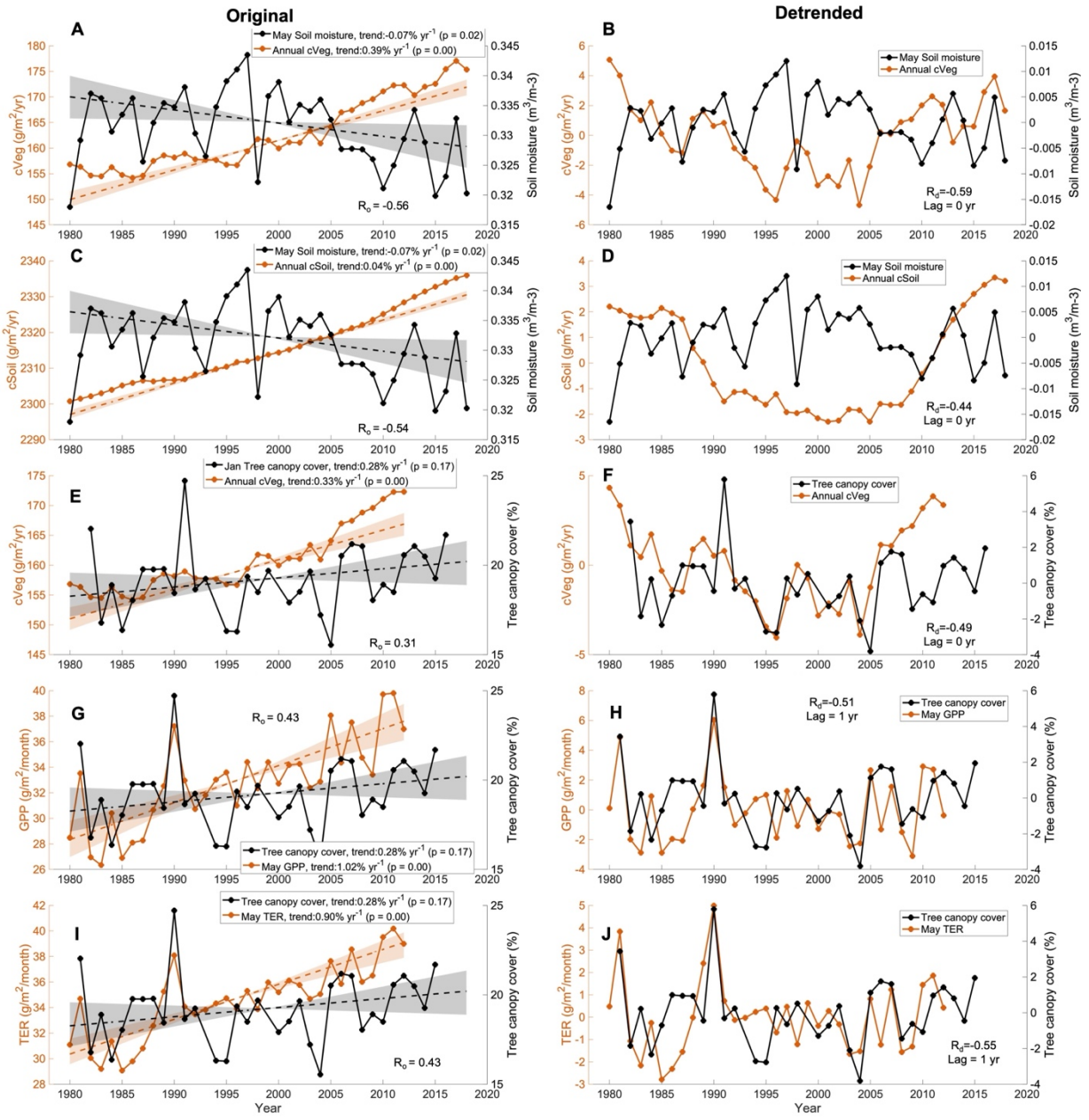

Fig. S9. Same as Fig. S5, except showing the covariation between annual vegetation carbon storage and May soil moisture (A, B), annual soil carbon storage and May soil moisture (C, D), annual vegetation carbon storage and tree canopy cover (E, F), May GPP and tree canopy cover (G, H), May TER and tree canopy cover (I, J).

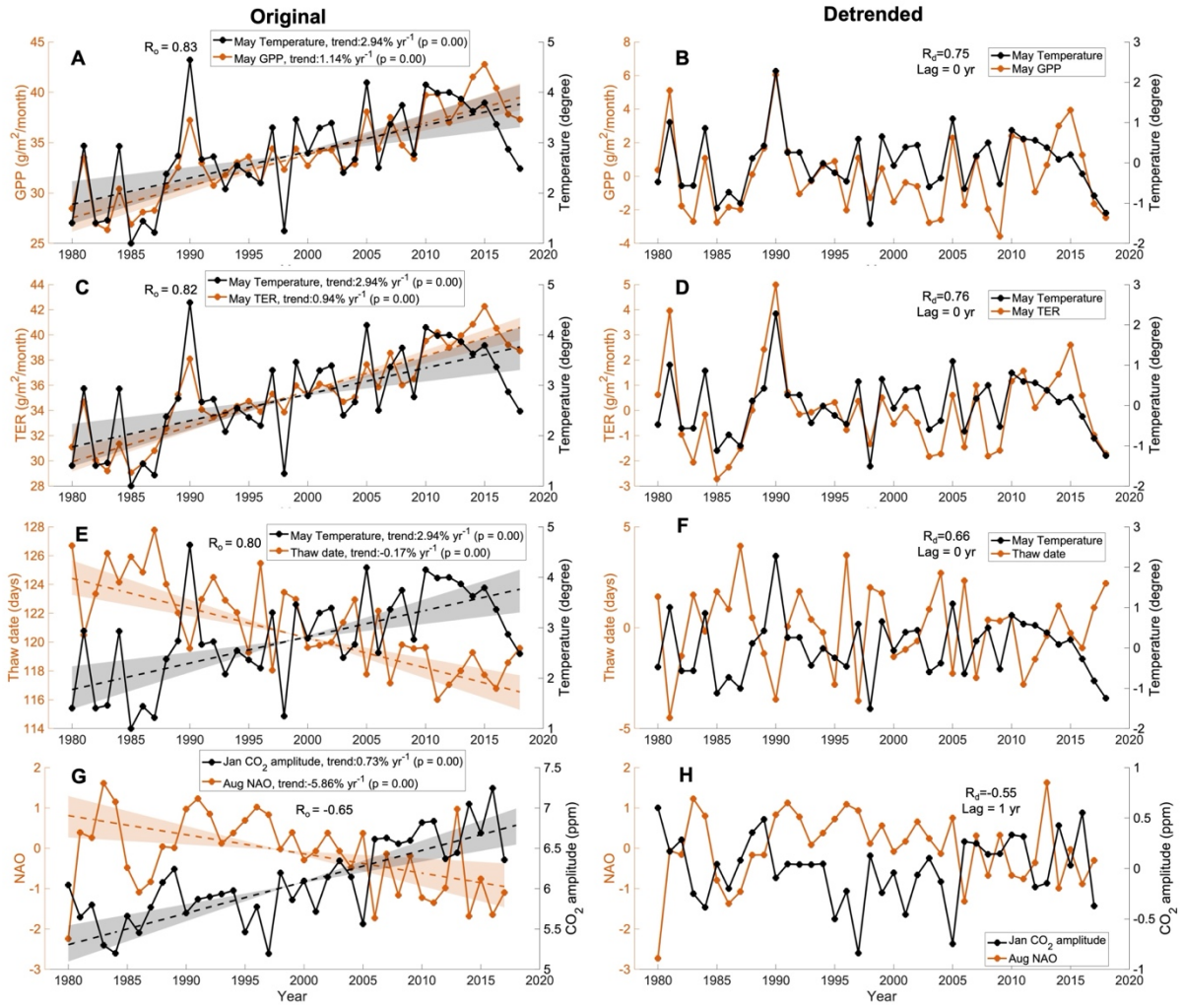

Fig. S10. Same as Fig. S5, except showing the covariation between May GPP and May temperature (A, B), May TER and May temperature (C, D), thaw date and May temperature (E, F), NAO and CO_2 amplitude (G, H).

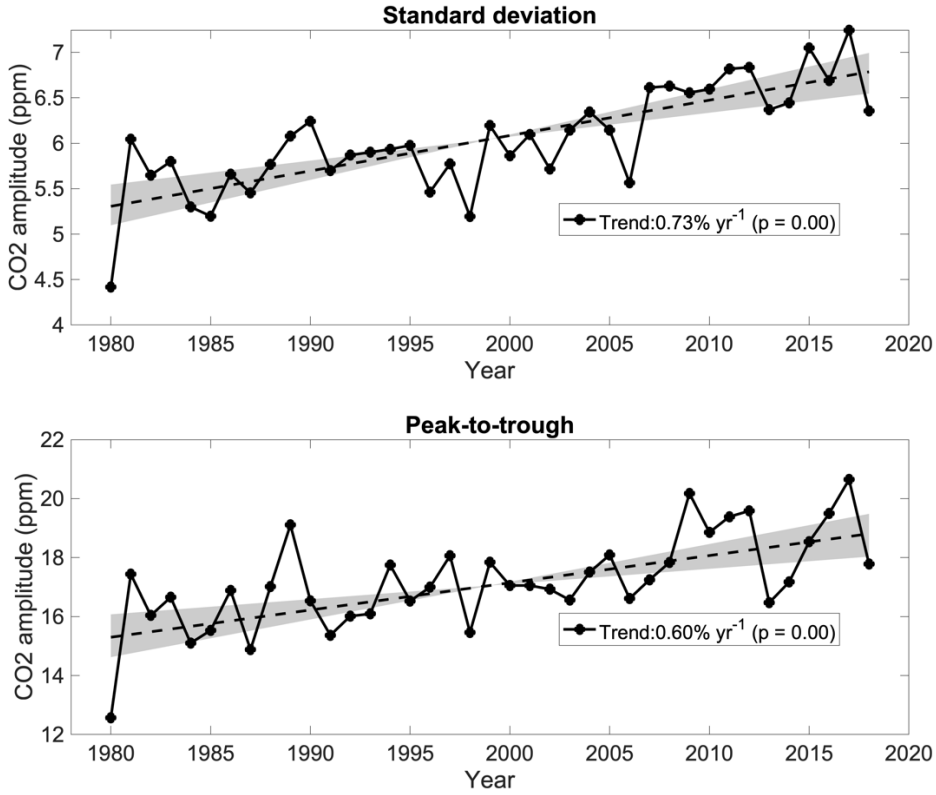

Fig. S11. Comparison of two methods for quantifying CO_2 amplitude. The upper panel shows CO_2 amplitude changes calculated using the standard deviation of each year, while the bottom panel shows CO_2 amplitude changes based on the peak-to-trough difference (maximum minus minimum). The Pearson correlation coefficient between the two time series is R = 0.85 (p=0.00).

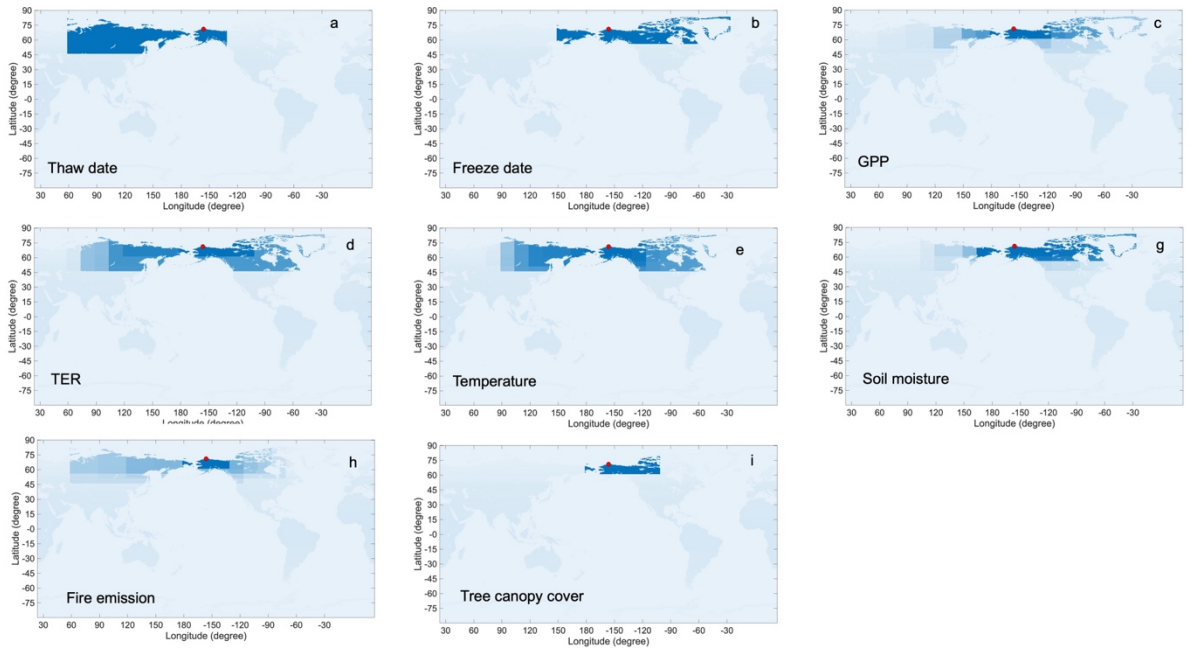

Fig. S12. Spatial domains of spatiotemporal variables most relevant to the footprint of CO_2 inter-annual variability. For variables including temperature (e), soil moisture (g), and fire emissions (h), the spatial domain for each month is determined, and each map displays the overlapping domain across all months. For GPP (c) and TER (d), the maps show the overlapping spatial domain across all months and all selected models. For variables with annual temporal scales, including thaw date (a), freeze date (b), and tree canopy cover (i), the spatial domains are derived from inter-annual variability. The red dot represents the location of Point Barrow.

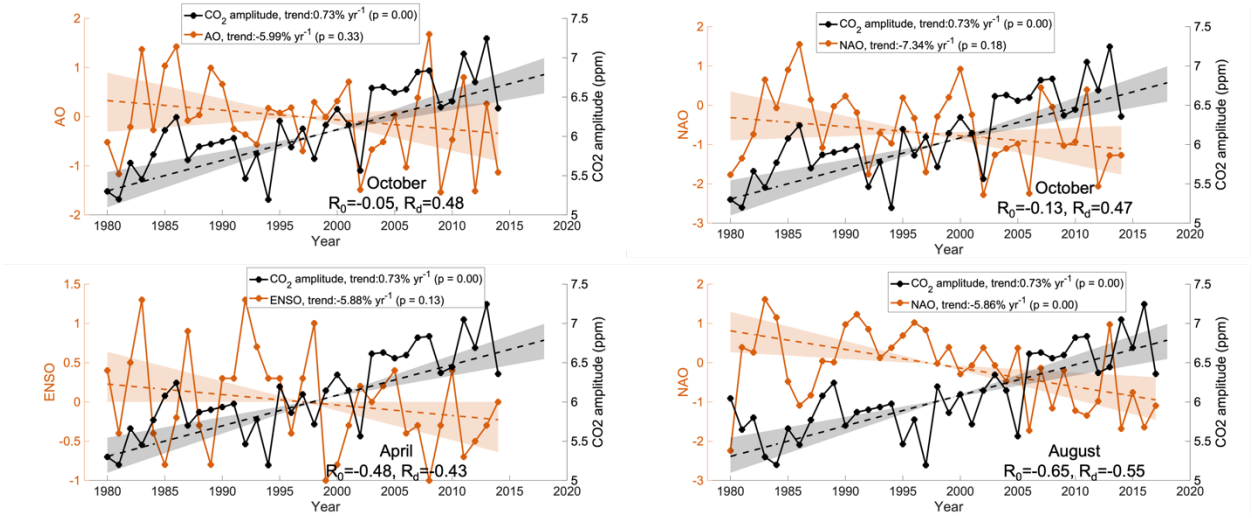

Fig. S13. Long-term changes in CO_2 amplitude, October AO and NAO, April ENSO, and August NAO in the period of 1980–2018. The long-term trend in October AO, April ENSO, and October NAO are insignificant ($p>0.05$) whereas the trend of August NAO is significant ($p<0.01$).

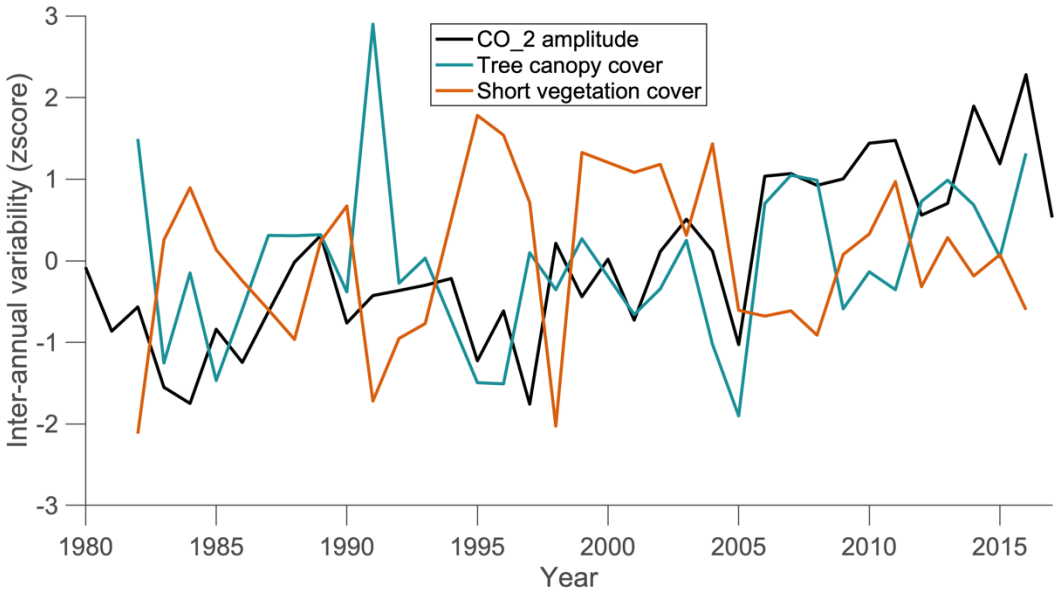

Fig. S14. Interannual variability (long-term trend removed) in annual CO_2 amplitude, tree canopy cover and short vegetation cover from 1980 to 2018.

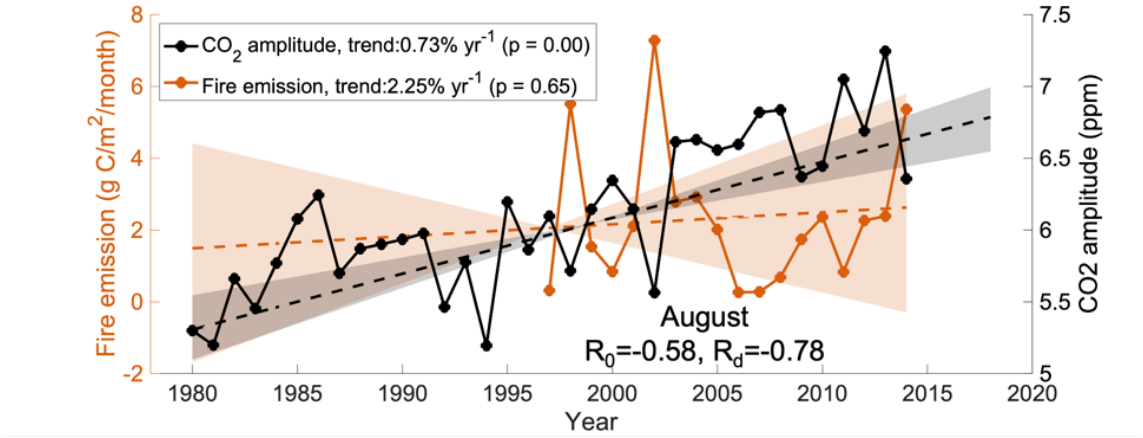

Fig. S15. Long-term changes in CO_2 amplitude (1980–2018) and fire emissions (1997–2018). Note that the fire emissions data from GFED4 have nearly two decades less temporal coverage than the CO_2 amplitude record, which limits confidence in both lag detection and assessment of long-term trends.

Table S1.

Pearson correlation between detrended CO_2 amplitude and GPP for each month from each selected TRENDY model. The last row presents the mean correlation value across all models.

	Jan	Feb	Mar	Apr	May	Jun	Jul	Aug	Sep	Oct	Nov	Dec
LPJmL	-0.53	0.15	0.41	-0.45	0.48	-0.03	0.07	-0.49	0.10	0.40	0.13	-0.53
CLASSIC	-0.33	0.21	-0.15	-0.53	0.43	0.12	-0.16	0.43	-0.07	0.46	-0.06	-0.32
CLM5.0	-0.41	-0.45	0.43	0.45	0.41	-0.11	0.56	0.58	0.45	0.41	-0.06	-0.42
DLEM	0.22	-0.03	0.34	0.46	0.22	0.13	0.00	0.33	0.10	0.45	0.23	0.29
IBIS	0.48	-0.22	0.45	-0.44	0.45	-0.45	-0.50	0.04	0.13	0.36	0.22	0.15
ISBA-CTRIP	0.46	-0.12	-0.41	0.35	0.47	0.13	-0.48	-0.52	0.07	0.42	0.20	-0.12
JSBACH	0.17	-0.27	0.38	0.37	0.05	-0.01	-0.51	-0.54	0.09	0.45	0.14	-0.20
JULES	0.20	-0.21	0.33	0.37	0.47	0.30	0.48	0.45	0.13	0.52	0.18	0.40
LPX-Bern	0.14	-0.23	0.32	-0.46	0.42	-0.05	0.10	-0.57	0.06	0.43	0.11	0.26
VISIT	0.71	NaN	0.98	0.32	0.45	0.06	-0.55	0.51	0.19	0.48	-0.54	-0.31
Mean value	0.11	-0.13	0.31	0.04	0.39	0.01	-0.10	0.02	0.12	0.44	0.05	-0.08

Table S2.

Pearson correlation between original CO_2 amplitude and GPP for each month from each selected TRENDY model. The last row presents the mean correlation value across all models.

	Jan	Feb	Mar	Apr	May	Jun	Jul	Aug	Sep	Oct	Nov	Dec
LPJmL	0.00	-0.05	0.45	0.24	0.78	0.74	0.59	0.61	0.62	0.04	0.32	0.07
CLASSIC	-0.05	0.58	0.19	0.22	0.65	0.67	0.75	0.76	0.56	0.50	0.50	-0.05
CLM5.0	-0.12	0.54	0.71	0.71	0.69	0.55	0.86	0.83	0.77	0.68	0.55	-0.10
DLEM	0.43	0.47	0.56	0.05	0.64	0.77	0.77	0.74	0.76	0.55	0.56	0.48
IBIS	0.22	-0.18	0.50	0.43	0.73	0.71	0.64	0.69	0.63	0.69	0.50	0.31
ISBA-CTRIP	0.25	0.08	-0.55	0.65	0.76	0.74	0.69	0.75	0.69	0.55	0.50	0.16
JSBACH	0.30	-0.06	0.40	0.61	0.54	0.63	0.54	0.59	0.62	0.55	0.55	0.04
JULES	0.42	0.02	0.51	0.66	0.76	0.77	0.84	0.83	0.73	0.74	0.57	0.48
LPX-Bern	0.08	-0.05	0.19	-0.44	0.59	0.58	0.62	0.63	0.63	0.54	0.31	0.34
VISIT	-0.05	1.00	-0.95	0.56	0.79	0.77	0.75	0.83	0.75	0.66	0.41	0.48
Mean value	0.15	0.23	0.20	0.37	0.69	0.69	0.70	0.73	0.68	0.55	0.48	0.22

Table S3.

Lag time between CO_2 amplitude and GPP for each month from each selected TRENDY model. Note that time series are detrended in the time lag analysis. The last row presents the mode value across all models. The value 999 indicates that there is no legacy effect between a pair of time series (see Method for the criteria).

	Jan	Feb	Mar	Apr	May	Jun	Jul	Aug	Sep	Oct	Nov	Dec
LPJmL	4	999	0	3	0	999	999	5	999	1	999	1
CLASSIC	999	999	999	4	1	999	999	3	999	3	999	999
CLM5.0	0	4	1	1	1	999	3	3	3	2	999	0
DLEM	999	999	999	5	999	999	999	999	999	2	999	999
IBIS	5	999	0	4	2	3	5	999	999	999	999	999
ISBA-CTRIP	5	999	4	999	0	999	5	5	999	2	999	999
JSBACH	999	999	999	999	999	999	5	5	999	2	999	999
JULES	999	999	999	999	0	999	2	2	999	2	999	4
LPX-Bern	999	999	999	0	0	999	999	5	999	2	999	999
VISIT	999	999	1	999	2	999	5	0	999	2	4	999
Mode value	999	999	999	999	0	999	999	999	999	2	999	999

Table S4.

Pearson correlation between detrended CO_2 amplitude and TER for each month from each selected TRENDY model. The last row presents the mean correlation value across all models.

	Jan	Feb	Mar	Apr	May	Jun	Jul	Aug	Sep	Oct	Nov	Dec
LPJmL	0.45	-0.40	0.17	-0.46	0.44	0.14	0.51	-0.64	0.10	0.52	0.17	0.42
CLASSIC	-0.04	-0.19	-0.16	0.43	0.49	0.11	0.42	-0.15	-0.11	0.51	-0.10	0.53
CLM5.0	-0.13	-0.48	0.40	-0.44	0.42	0.04	-0.05	0.54	0.46	0.54	-0.07	0.50
DLEM	-0.46	-0.55	0.35	-0.41	0.46	-0.13	0.40	-0.48	0.08	0.49	0.26	-0.43
IBIS	0.25	0.02	0.34	0.33	0.46	0.01	-0.41	0.21	0.10	0.52	0.15	0.01
ISBA-CTRIP	0.18	-0.42	0.37	0.39	0.48	-0.48	0.53	-0.52	0.00	0.50	0.17	0.43
JSBACH	0.41	-0.43	0.34	0.47	0.48	0.24	0.41	-0.54	0.08	0.48	-0.10	0.52
JULES	0.16	-0.03	0.30	0.38	0.42	0.26	0.49	-0.48	0.04	0.56	0.14	0.28
LPX-Bern	0.02	-0.43	0.40	0.43	0.50	0.18	0.03	-0.56	0.04	0.57	0.55	0.45
VISIT	0.27	-0.44	0.35	0.37	0.45	0.04	-0.42	0.47	0.15	0.62	0.09	0.01
Mean value	0.11	-0.33	0.29	0.15	0.46	0.04	0.19	-0.21	0.09	0.53	0.13	0.27

Table S5.

Pearson correlation between original CO_2 amplitude and TER for each month from each selected TRENDY model. The last row presents the mean correlation value across all models.

	Jan	Feb	Mar	Apr	May	Jun	Jul	Aug	Sep	Oct	Nov	Dec
LPJmL	0.54	0.24	0.35	0.40	0.77	0.77	0.81	0.70	0.67	0.66	0.56	0.56
CLASSIC	0.40	0.62	0.03	0.67	0.75	0.74	0.76	0.71	0.61	0.61	0.61	0.78
CLM5.0	0.56	0.63	0.73	0.45	0.72	0.73	0.69	0.79	0.77	0.72	0.62	0.72
DLEM	0.34	0.19	0.45	0.47	0.70	0.73	0.81	0.77	0.74	0.62	0.59	0.23
IBIS	0.45	0.25	0.58	0.69	0.75	0.65	0.70	0.72	0.64	0.79	0.57	0.51
ISBA-CTRIP	0.51	0.42	0.59	0.68	0.80	0.67	0.83	0.71	0.73	0.70	0.64	0.69
JSBACH	0.62	0.36	0.60	0.72	0.78	0.76	0.77	0.64	0.69	0.76	0.48	0.76
JULES	0.34	0.18	0.53	0.65	0.71	0.75	0.75	0.74	0.70	0.76	0.59	0.57
LPX-Bern	0.33	0.52	0.57	0.66	0.75	0.61	0.75	0.73	0.67	0.75	0.81	0.72
VISIT	0.33	0.28	0.44	0.65	0.79	0.67	0.72	0.81	0.72	0.83	0.53	0.52
Mean value	0.44	0.37	0.49	0.60	0.75	0.71	0.76	0.73	0.69	0.72	0.60	0.61

Table S6.

Lag time between CO_2 amplitude and TER for each month from each selected TRENDY model. Note that time series are detrended in the time lag analysis. The last row presents the mode value across all models. The value 999 indicates that there is no legacy effect between a pair of time series (see Method for the criteria).

	Jan	Feb	Mar	Apr	May	Jun	Jul	Aug	Sep	Oct	Nov	Dec
LPJmL	5	3	999	4	0	999	1	5	999	2	999	2
CLASSIC	999	999	999	1	1	999	3	999	999	3	999	3
CLM5.0	999	4	1	4	1	999	999	3	5	3	999	3
DLEM	3	3	999	4	2	999	2	5	999	2	999	4
IBIS	999	999	999	999	2	999	3	999	999	2	999	999
ISBA-CTRIP	999	3	999	999	0	5	1	5	999	2	999	2
JSBACH	5	3	999	0	0	999	1	5	999	2	999	2
JULES	999	999	999	999	0	999	1	5	999	2	999	999
LPX-Bern	999	5	999	0	0	999	999	5	999	2	2	2
VISIT	999	3	999	999	2	999	5	0	999	2	999	999
Mode value	999	3	999	999	0	999	999	999	999	2	999	999